Force sensing with an optomechanical system at room temperature

Ze Feng Yan,[1] Bing He,[2,*] and Qing Lin[1,†]

[1]*Fujian Key Laboratory of Light Propagation and Transformation & Institute of Systems Science, College of Information Science and Engineering, Huaqiao University, Xiamen 361021, China*

[2]*Center for Quantum Optics and Quantum Information, Universidad Mayor, Camino La Pirámide 5750, Huechuraba, Chile*

(Received 23 August 2022; revised 29 November 2022; accepted 17 January 2023; published 30 January 2023)

We present an alternative approach to force sensing with optomechanical systems. The operation is based on a nonlinear dynamical mechanism, which locks the mechanical oscillation and the associated cavity field pattern of a system when two external drive tones satisfy a frequency match condition. Under a weak force that adds a slight detuning to the external driving fields, the cavity field will undergo a transition between two locked patterns while the locked mechanical oscillation is well preserved, thus having the small modifications to its sidebands. The force sensing is realized by detecting the intensity changes of the cavity field sidebands in such process. With the currently available optomechanical systems, the sensitivity of force detection can reach the level of attonewton and can be further improved with improved system parameters and longer detection time. One important feature of the applied dynamical scenario is that thermal noise insignificantly affects the cavity field sidebands of the locked states, so that the scheme can work well even at room temperature. This method is hopeful to reduce the difficulty in the practical applications of force sensing.

DOI: 10.1103/PhysRevA.107.013529

I. INTRODUCTION

How to measure a physical quality as accurately as possible is highly important to both fundamental research and practical applications. Nowadays sensing is a widely applied technology in almost every aspect of daily life, including mass, size, force, acceleration, and so on [1,2]. Thanks to its tiny mass and ultrahigh mechanical frequency, a nanomechanical resonator is usually used for mass sensing with ultrahigh resolution. For instance, yoctogram resolution can be achieved with the GHz nanomechanical resonator [3]. For size sensing, the whispering gallery mode microcavity is regarded as a good candidate since it has an ultrahigh quality factor and small mode volume [4,5]. Dozens of nm resolution can be achieved with mode shift [6], mode splitting [7], or mode broadening [8].

In this work, we will study a method for force sensing, which aims to detect an extremely low magnitude of static force. Force sensing used to be performed with hybrid systems. So far, various experiments [9–12] and theoretical schemes [13–28] were reported to realize the force sensing to different levels. In 2012, Gavartin *et al.* combined a nanomechanical beam with a microdisk cavity in an integrated hybrid system to achieve a sensitivity 74 aN/$\sqrt{\text{Hz}}$ under room temperature by the comparison of averaged probe phase fluctuations with and without external force [9]. If the average measurement time is as long as 35 seconds, the sensitivity of the setup can be increased to 15 aN/$\sqrt{\text{Hz}}$. Later, in 2013, Moser *et al.* used a carbon nanotube as the mechanical resonator and realized the sensitivity of 12 zN/$\sqrt{\text{Hz}}$ at the temperature of 1.2 K by the detection of the mechanical motion of the carbon nanotube induced by the resonant periodic force [10]. Afterward, in 2014, Schreppler *et al.* injected the ultracold atom gas into an optical F-P cavity. When the external force resonated with the oscillation frequency of the cloud, the sensitivity 42 ± 13 yN/$\sqrt{\text{Hz}}$ near the standard quantum limit (SQL) was realized by the heterodyne detection of phase fluctuations of probe light [11]. Later, in 2016, Buchmann *et al.* suggested realizing force sensing beyond the SQL by the detection of complex correlations between the amplitude and phase fluctuations through so-called synodyne detection in an optomechanical system (OMS) [18]. More recently, Mason *et al.* inserted a thin Si_3N_4 membrane into the F-P cavity and achieved the sensitivity of 11.2 aN/$\sqrt{\text{Hz}}$, 1.5 dB below the SQL by exploiting strong quantum correlations through the measurement of a rotated quadrature at the temperature of 10 K [12].

Nonetheless, most of the experiments or theoretical schemes demand complicated hybrid structures and na ultra-low temperature environment, thus increasing the implementation difficulty and limiting their application feasibility. Here, we present a different approach of force sensing based on a nonlinear mechanism of optomechanics. Our scheme is simple, without a complicated structure, and can work well at room temperature. The high sensitivity to the aN-level is possible with the currently available experimental conditions and it can be improved further with a longer detection time or better system parameters.

The rest of the paper is organized as follows. In Sec. II, we give a detailed description of the dynamics of the concerned system. After that, in Sec. III, the mechanism of our weak force measurement is presented in detail. The different

*bing.he@umayor.cl
†qlin@hqu.edu.cn

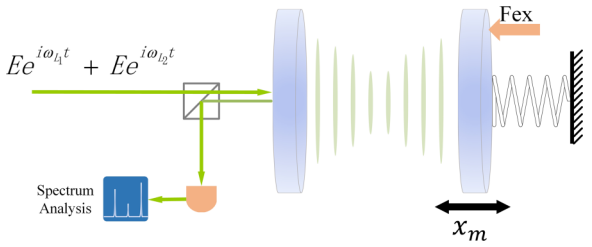

FIG. 1. The setup of the force sensor. A laser beam with two frequency components of different frequencies drives an optical cavity with a movable mirror. When an external constant force is applied to this mirror, the size of the cavity will be slightly changed. Through the detection of the changed amplitude of the cavity sidebands, this external force can be measured. Here the real displacement is related to the dimensionless displacement X_m as $x_m(t) = \sqrt{\hbar/(m\omega_m)}X_m(t)$, where m is the effective mass of the moving mirror.

features in the performance of the force detection are illustrated in Sec. IV. Finally, we discuss the experimental feasibility in Sec. V and conclude the work in Sec. VI.

II. SETUP AND ITS DYNAMICS

We consider a typical optomechanical system driven by a two-tone laser field with its frequency components ω_{L_1} and ω_{L_2}, which correspond to the two detunings $\Delta_1 = \omega_c^0 - \omega_{L_1}$ and $\Delta_2 = \omega_c^0 - \omega_{L_2}$ where ω_c^0 is the resonant cavity frequency with a fixed end mirror; see Fig. 1. The system dynamical equations in the rotation frame with respect to ω_c^0 can be expressed in terms of the dimensionless cavity quadratures X_c, P_c, together with the dimensionless mechanical displacement X_m, momentum P_m, as follows:

$$\begin{aligned}
\dot{X}_c &= -\kappa X_c - g_m X_m P_c + \sum_{i=1}^{2} \sqrt{2}[E_i + \sqrt{\kappa}\xi_i(t)]\cos(\Delta_i t),\\
\dot{P}_c &= -\kappa P_c + g_m X_m X_c + \sum_{i=1}^{2} \sqrt{2}[E_i + \sqrt{\kappa}\xi_i(t)]\sin(\Delta_i t),\\
\dot{X}_m &= \omega_m P_m,\\
\dot{P}_m &= -\omega_m X_m - \gamma_m P_m + g_m\left(X_c^2 + P_c^2\right)/2 - f_{ex}\\
&\quad + \sqrt{2\gamma_m}\xi_m(t),
\end{aligned} \tag{1}$$

where κ and γ_m are the damping rate of the cavity and mechanical modes, respectively. The cavity noise component $\sqrt{\kappa}\xi_{1(2)}(t)$ comes from the fluctuation of drive amplitude $E_{1(2)}$, and it can be well suppressed with the locked laser power. Meanwhile, the mechanical noise $\sqrt{2\gamma_m}\xi_m(t)$ comes from the coupling of the mechanical resonator to the thermal environment, and is determined by the correlation $\langle\xi_m(t)\xi_m(t')\rangle = n_{\rm th}\delta(t-t')$ with the thermal occupation $n_{\rm th} = 1/(e^{\hbar\omega_m/k_BT} - 1)$ [29] (the connection with the more general correlation for the thermal noise can be seen, e.g., in Ref. [30]). All of the nonlinear terms $-g_m X_m P_c$, $g_m X_m X_c$ and $g_m(X_c^2 + P_c^2)/2$ in the equations, where the single photon coupling strength is g_m, arise from the interaction between the cavity and mechanical modes in the form of radiation pressure. Moreover, the force term f_{ex} is proportional to the unknown one F_{ex} applied to the mechanical resonator.

Without loss of generality, the intensities of two drive fields can be set to be the same ($E_1 = E_2$). The different drive intensities will not bring any obvious difference in our concerned approach. When a weak constant force F_{ex} is applied to the movable mirror, the cavity length L will be changed accordingly. Supposed that the cavity length is reduced from L to $L - \delta L$, the corresponding resonance frequency of the cavity mode will be accordingly modified to

$$\begin{aligned}
\omega_c^0 &= k\frac{\pi c}{L}\\
\rightarrow \omega_c &= \frac{k\pi c}{L - \delta L}\\
&\sim \omega_c^0(1 + \delta L/L),
\end{aligned} \tag{2}$$

where k is the integer mode number. With such a relative shift of the cavity frequency $\delta_F/\omega_c^0 = \delta L/L$, the detunings of the two driving fields will undergo the change

$$\begin{aligned}
\Delta_1 &\rightarrow \Delta_1 + \delta_F,\\
\Delta_2 &\rightarrow \Delta_2 + \delta_F.
\end{aligned} \tag{3}$$

These shifts change the quadratures X_c and P_c in Eq. (1), which could be measured directly as proposed previously [31], but we will make use of the corresponding change in the cavity-field spectrum amplitudes for the measurements.

III. MECHANISM FOR FORCE SENSING

We first look at the situation of a single driving field. The radiation pressure from the driving laser gives rise to the optomechanical interaction between the cavity and mechanical modes. When the drive detuning Δ is away from the red-detuned resonant point ($\Delta = \omega_m$), the mechanical motion enters a stable oscillation

$$X_m = A_m\cos(\omega_m t) + d_m, \tag{4}$$

given a strong enough drive intensity [32,33]. The corresponding cavity field, $\alpha(t) = [X_c(t) + iP_c(t)]/\sqrt{2}$ will have a form Fourier series

$$\alpha(t) = e^{i\phi(t)}\sum_n \alpha_n e^{i(n\omega_m + \Delta)t}, \tag{5}$$

where $\phi(t) = g_m A_m/\omega_m \sin(\omega_m t)$ (n is the integer). The Fourier components α_n can be found analytically as

$$\alpha_n = \frac{E}{\kappa}\frac{J_n(-g_m A_m/\omega_m)}{in\omega_m/\kappa + 1 - i(g_m d_m - \Delta)/\kappa}, \tag{6}$$

where $J_n(x)$ is the Bessel function of the first kind.

The peaks of the cavity field spectrum [the Fourier series in Eq. (5)] will be shifted after an external force is applied to have the shift δ_F. Such a shift δ_F is similar to the term $g_m d_m$ in the denominator of Eq. (6). In principle, the detection of a tiny frequency shift of the cavity field spectrum components can be performed by a careful measurement under the condition of a stable driving laser frequency, which guarantees that the small shift δ_F should not be indistinguishable from the drive frequency fluctuation. This practice could be hard to implement for a shift much less than the cavity line width κ. In

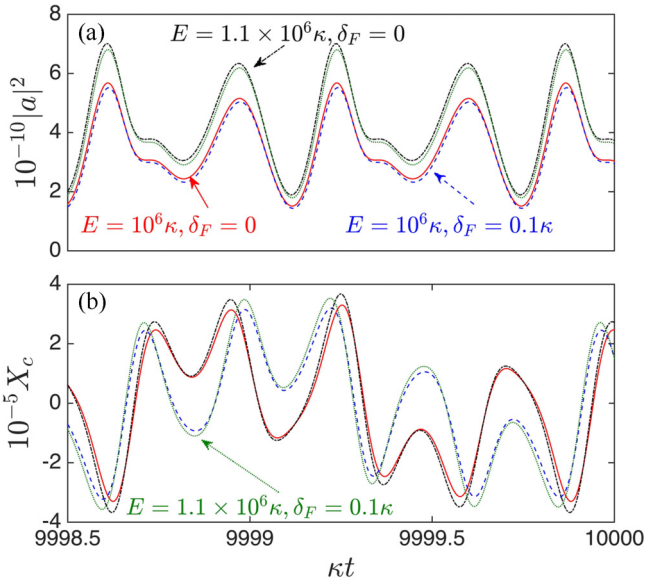

FIG. 2. The stabilized cavity field intensity as the photon number $|a|^2$ and the stabilized pattern of the field quadrature X_c in the time domain. While the cavity oscillation pattern is locked under the frequency match condition for two driving fields, the $|a|^2$ for the exemplary drive amplitudes $E = 10^6\kappa$ to $E = 1.1 \times 10^6\kappa$ become similar. A frequency shift $\delta_F = 0.1\kappa$ induced by the external force modifies the field spectrum to deviate the $|a|^2$ from the original ones. It is more obvious to see the modified quadrature X_c (in the system rotating at the resonant cavity frequency) due to the shift δ_F. The parameters are chosen as $g_m = 10^{-5}\kappa$, $\omega_m = 10\kappa$, which are scaled with the field damping rate κ and $Q = \omega_m/\gamma_m = 10^4$.

a realistic experiment, one can detect a small frequency shift (up to $10^{-3}\kappa$) based on the stabilized driving laser frequency by the Pound-Drever-Hall (PDH) technique [34–36].

The purpose of our current work is to present an alternative approach to measure the shift $\delta_F < \kappa$. Figure 2 illustrates the basic mechanism for the measurement, where an OMS is driven by two driving fields under the frequency condition

$$|\Delta_2 - \Delta_1| = \omega_m. \tag{7}$$

Under such a condition the mechanical oscillation demonstrates particular behaviors as compared with the situations of only one driving laser field. This difference can be understood from the stabilized cavity field in the time domain. When the frequencies of two laser drives well satisfy the match condition in Eq. (7), an optomehcanical nonlinearity will be enhanced so that the amplitude and phase of the mechanical resonator will be fully locked, irrespective of the change of drive amplitude E [37,38]. Meanwhile, the cavity-field pattern (the distribution of the frequency components) will be locked as well, but the associated amplitudes of the sidebands vary proportionally with the drive amplitude E. This character can be seen from the stabilized cavity intensity equivalent to the intracavity photon number $|a|^2 = (X_c^2 + P_c^2)/2$ or the stabilized cavity-field quadrature X_c for the different $E = 10^6\kappa$ (the red solid curve) and $E = 1.1 \times 10^6\kappa$ (the black dash-dotted curve) in Fig. 2. As seen from the simulated results in Fig. 2, the black dash-dotted curve and the red solid curve are similar (proportional to each other) because they

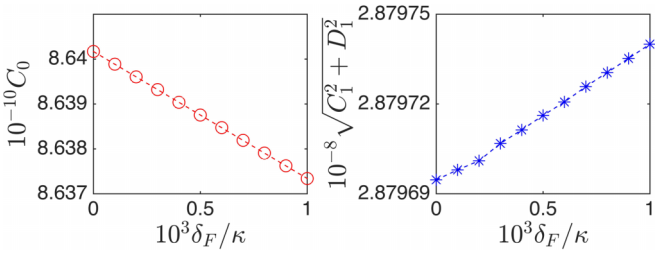

FIG. 3. The variations of the zeroth- and first-order sideband with the detuning induced by an external force. The system parameters are the same as those in Fig. 2, and the drive amplitude is kept to be $E = 1.1 \times 10^6\kappa$.

have the same spectrum pattern but different amplitudes of the frequency components. When an external force is applied, the induced frequency shift δ_F changes the effective detuning of the two drives simultaneously, such that the match condition in Eq. (7) is still satisfied. Therefore, the blue-dashed and green-dotted curves in Fig. 2 are also similar, indicating that the amplitude and phase of the mechanical resonator will be still locked after a shift δ_F. However, such a shift of drive detuning will modify the cavity field spectrum from the original one to another, e.g., the transition from the red-solid curve to the blue-dashed curve in Fig. 2. Such redistribution of cavity sidebands, manifesting as the modifications of the real-time cavity field shown in Fig. 2, can be sufficiently perceivable to realize a measurement with high resolution.

One choice is with the real-time cavity photon number

$$|a(t)|^2 = \sum_l \left\{ \int d\omega C_l(\omega) \cos(\omega t) + \int d\omega D_l(\omega) \sin(\omega t) \right\}, \tag{8}$$

where $C_l(\omega)$ and $D_l(\omega)$ are peaked at $\omega = l\omega_m$ ($l \geqslant 0$). Under two simultaneous driving fields, it is impossible to have an analytical form of the above like the one in Eqs. (5) and (6), but the Fourier components C_l and D_l can be found numerically with the evolved $|a(t)|^2$. Figure 3 displays the changes of two components C_0 at $\omega = 0$ and $\sqrt{C_1^2 + D_1^2}$ at $\omega = \omega_m$, which determine the pure displacement d_m and the oscillation amplitude A_m in Eq. (4), respectively. Due to the linear resonance effect, the high-order sidebands of $|a(t)|^2$ ($l \geqslant 2$) have a negligible effect on the mechanical motion. The pure displacement d_m in Eq. (4), for example, is decided by three forces, the radiation pressure proportional to the component C_0, the spring restoring force proportional to the displacement d_m itself, as well as the measured external force proportional to δ_F. A relation demonstrated in Fig. 3 indicates how the radiation pressure is lowered by the balance of these forces at the equilibrium point (the spring force and radiation pressure are opposite to the external force).

We here adopt another approach based on the cavity field

$$\begin{aligned} a(t) &= \frac{1}{\sqrt{2}}[X_c(t) + iP_c(t)] \\ &= \frac{1}{\sqrt{2}} \sum_n \left\{ \int d\omega A_n(\omega) \cos(\omega t) + i \int d\omega B_n(\omega) \sin(\omega t) \right\}. \end{aligned} \tag{9}$$

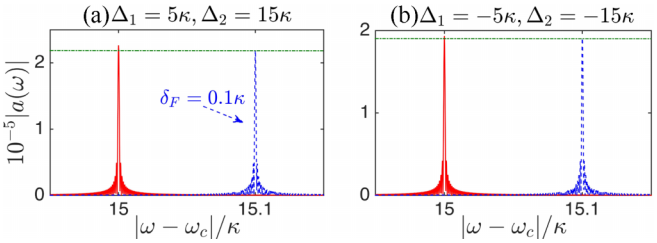

FIG. 4. The first-order cavity field sideband under two different detuning combinations. Here the different combinations (Δ_1, Δ_2) indicate the frequencies of the two used driving fields and the sideband at the position ω_1, which is defined in Eq. (10), is measured for both combinations. After the shift $\delta_F = 0.1\kappa$, the sideband peak shifts from the red solid one to the blue dashed one, associated with a decrease of the amplitude (the green dash-dotted lines delineate the amplitude change). The parameters are chosen to be the same as those in Fig. 2 and the drive amplitude is set to be $E = 10^6\kappa$.

Each component of $|a(t)|^2$ in Eq. (8) comes from the contributions of all terms in the above, so that the behaviors of $A_n(\omega)$ and $B_n(\omega)$ are different from those of $C_n(\omega)$ and $D_n(\omega)$. Here in Fig. 4, the two examples of the first cavity field sideband are with $\Delta_1 = 5\kappa$, $\Delta_2 = 15\kappa$, and $\Delta_1 = -5\kappa$, $\Delta_2 = -15\kappa$, respectively. Though the analytical solution of the cavity field under two driving fields is not available, the field spectrum can be still analyzed numerically to find its components peaked around $n\omega_m + |\Delta_1|$, similar to the ones in Eq. (6). Under the condition $|\Delta_2 - \Delta_1| = \omega_m$, the sidebands are enhanced by the contributions from two different driving fields. When an external force is applied to induce a frequency shift, say $\delta_F = 0.1\kappa$, the sidebands are shifted accordingly as shown in Fig. 4. A different feature from the scenarios of a single drive is that the amplitude of a sideband will be modified together with its frequency shift. Such amplitude changes are proportional to the shifts δ_F, providing a possible way to detect the external force.

IV. FORCE SENSING PERFORMANCE

A. Force-response relation

The first point one needs to know about the force sensing performance is how the measured quantity varies with the external force to be measured. To avoid possible confusion, we adopt the following notation:

$$\omega_n = n\omega_m + |\Delta_1|, \tag{10}$$

where the integer $n \geqslant 1$ is the order of the sidebands for the positions of all cavity field sidebands in Eq. (9). The corresponding sideband intensity

$$n_c^{(n)}(\omega_n) = A_n^2(\omega_n) + B_n^2(\omega_n), \tag{11}$$

can be measured precisely through the input-output relation

$$a_{\text{out}}(t) = a_{\text{in}}(t) - \sqrt{\kappa}a(t). \tag{12}$$

We choose to work with the second-order sideband ($n = 2$) because its intensity change is even larger. The correlation between the sideband intensity change $\delta n_c^{(2)} = |n_c^{(2)}(\omega_2 + \delta_F) - n_c^{(2)}(\omega_2)|$ and the shift δ_F is shown in Fig. 5, where the linear relation proves that a good scaling between the measured $\delta n_c^{(2)}$ and the force that induces the $\delta n_c^{(2)}$ can be well established. This linear relation is highly beneficial to the measurement of unknown external forces.

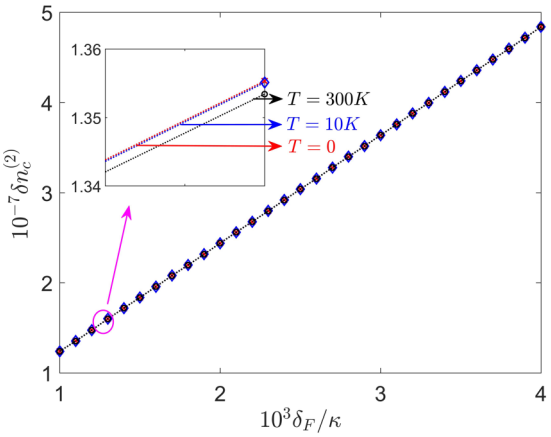

FIG. 5. The relations between the sideband intensity changes and the induced shifts δ_F at different temperature. The mechanical quality factor is fixed to be $Q = 10^4$ and the sideband intensity difference is slightly modified by the increased temperature. The combination of the two driving frequencies is $\Delta_1 = -5\kappa$, $\Delta_2 = -15\kappa$, while the drive amplitude is $E = 1.1 \times 10^6\kappa$. We here measure the sideband at ω_2 defined in Eq. (10). The fixed parameters are the same as those in Fig. 2.

B. Uncertainty in measurement

In a real experiment the measurement accuracy is limited by the shot noise due to a statistics property. Therefore, we define the following signal-to-noise ratio (SNR)

$$\text{SNR} = \frac{\left|n_{c,\text{out}}^{(2)}(\omega_2; t_d) - n_{c,\text{out}}^{(2)}(\omega_2 + \delta_F; t_d)\right|}{\sqrt{n_{c,\text{out}}^{(2)}(\omega_2; t_d)} + \sqrt{n_{c,\text{out}}^{(2)}(\omega_2 + \delta_F; t_d)}}, \tag{13}$$

as a figure of merit to discriminate the intensity change due to the frequency shift δ_F. What is measured according to Eq. (12) is a flux of photons proportional to κ in the unit Hz, so the measured spectrum change $n_{c,\text{out}}^{(2)}(\omega_2; t_d)$ is an accumulated amount over the measurement time t_d. Without loss of generality we set a detection time $t_d = 1$ s.

It is clear that the drive intensity is an important system parameter relevant to the intensity change. Taking the currently available experimental conditions into account, we select a range of the drive intensity from $E = 5 \times 10^5\kappa$ to $1.1 \times 10^6\kappa$ (the drive power is within 1 W for the optical drive frequencies). Figure 6(a) displays the relations between the SNR and the driving field amplitude E for three different detuning combinations under a fixed frequency shift $\delta_F = 5 \times 10^{-3}\kappa$. The SNR with the two drive frequencies whose detuning is far away from the resonant point (the red and blue ones) is obviously larger than the one due to the combination with one resonant drive frequency (the black one). This is because the nonlinear interaction between the cavity mode and the mechanical mode, which determines the cavity-field spectrum, becomes the strongest when it is driven at the resonant point. Since the frequency shift induced by the external force is so tiny as $\delta_F = 5 \times 10^{-3}\kappa$, the

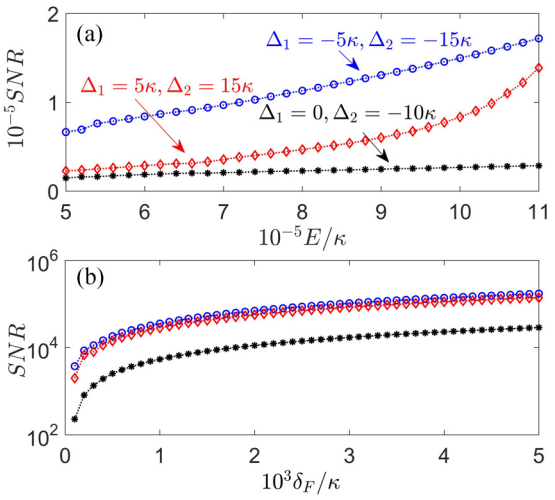

FIG. 6. (a) The SNR versus the drive amplitude E/κ. The frequency shift is assumed to be $\delta_F = 5 \times 10^{-3}\kappa$ and the difference in the drive amplitude between two neighboring points in the figure is fixed to be $2 \times 10^4\kappa$. These results indicate the SNR for three different combinations (Δ_1, Δ_2), where $|\Delta_1 - \Delta_2| = \omega_m$. For all these combinations we measure the sideband at the locations of ω_2 defined in Eq. (10). (b) The SNR versus the frequency shift δ_F/κ. The drive amplitude is fixed to be $E = 1.1 \times 10^6\kappa$, and the difference of the frequency shift between two neighboring points in the figure is $\delta_F = 10^{-4}\kappa$. The SNR also increases linearly with the increasing of frequency shift (a logarithmic scale is used for the vertical axis). The fixed parameters are the same as those in Fig. 2.

amplitude change of the second-order sideband is less obvious under the strongest optomechanical interaction. On the other hand, the optomechanical interaction is relatively weak at the off-resonant point, e.g., $\Delta_1 = -5\kappa$ and $\Delta_2 = -15\kappa$. Especially when the detuning is farther away from the resonant point, e.g., $\Delta_1 = -8\kappa$ and $\Delta_2 = -18\kappa$, the optomechanical interaction will be even weaker, losing the amplitude and phase locking for the mechanical oscillation unless the drive amplitude E is enhanced to compensate for the weakened cavity field. In this case, a tiny frequency shift induced by external force (under a fixed drive amplitude E) will bring about more obvious modification to the cavity-field spectrum. For the comparison between the blue-detuned combination $\Delta_1 = -5\kappa$, $\Delta_2 = -15\kappa$ and the red-detuned one $\Delta_1 = 5\kappa$, $\Delta_2 = 15\kappa$, the first leads to the higher intensities $n^{(2)}_{c,\mathrm{out}}(\omega_2; t_d)$ and $n^{(2)}_{c,\mathrm{out}}(\omega_2 + \delta_F; t_d)$ in Eq. (13) to realize a higher SNR.

To a force sensor, the range of the weak forces to be detected is another important figure of merit. In Fig. 6(b), we fix the drive intensity at $E = 1.1 \times 10^6\kappa$ and vary the frequency shift from $\delta_F = 10^{-4}\kappa$ to $\delta_F = 5 \times 10^{-3}\kappa$ by a step $10^{-4}\kappa$. Over this range of the shifted detuning, the SNR for the different drive combinations vary so dramatically that we need to use a logarithmic scale for the illustrated SNR. We find that high SNR can be achieved over a considerable range of the frequency shift δ_F so that the force sensor can work well to detect a wide range of weak forces.

Based on the above results, we can estimate the sensitivity of our scheme under the currently available experimental conditions. The SNR for a frequency shift $\delta_F = 5.0 \times 10^{-3}\kappa$ is about 1.72×10^5 given the drive amplitude $E = 1.1 \times 10^6\kappa$ and the detunings $\Delta_1 = -5\kappa$, $\Delta_2 = -15\kappa$ in Fig. 6(a). The corresponding laser power is about 157 mW with the wavelength around $\lambda = 1537$ nm. If one regards SNR = 1 as the detection limit, the minimum frequency shift $\delta_{F,\min} = 2.9 \times 10^{-8}\kappa$ can thus be discriminated under such conditions. In practice, a cavity with its length $L = 1$ mm and a finesse 9.4×10^5 (corresponding to the damping rate $\kappa = 1$ MHz), together with a mechanical resonator with a mass $m = 10^{-12}$ kg and frequency $\omega_m = 10$ MHz, is feasible to be fabricated with the current experimental technology [33]. Therefore, the limit of a weak force that can be detected is

$$\begin{aligned} F &= m\omega_m^2 \delta L \\ &= m\omega_m^2 \left(L/\omega_c^0\right)\delta_{F,\min} \\ &= 2.4 \times 10^{-18} N, \end{aligned} \tag{14}$$

i.e., at the level of attonewton. This sensitivity can be further improved with the system parameters. For example, if we increase the finesse by one order (9.4×10^6), the required laser power can be reduced to be 15.7 mW and the limit of the detected weak force can be decreased to $7.6 \times 10^{-20} N$.

C. Robustness against thermal noise

In a realistic environment of nonzero temperature, the system is coupled to the thermal environment and the associated thermal noise can considerably influence the system dynamics, especially in the measurements at the quantum level. For this reason, most precise measurement schemes require an ultra-low-temperature environment for their performance, as the examples in Refs. [10–12,18]. Such a requirement limits the applicability of those force sensing schemes.

An advantage of the dynamical scenario under two driving fields satisfying the condition in Eq. (7) is that the mechanical oscillation can be completely locked without changing it amplitude and phase even if the drive power is varied within a certain range [37,38]. Meanwhile, the noise perturbations can hardly affect such a locked mechanical oscillation as well. This feature can facilitate the performance of the force sensing at room temperature. In the numerical calculations, we can apply a random function generated with MATLAB to simulate the thermal noise drive term $\sqrt{2\gamma_m}\xi_m(t)$ in Eq. (1).

The thermal noise only adds small corrections to the evolved cavity fields as shown in Fig. 7 since the contributions from the coherent pumps always dominate. However, a detailed comparison between the noise corrections $\delta|a|^2$ due to the thermal noise explains why the scenario of two drives is better for a precise measurement. Compared to the $\delta|a|^2$ existing in a singly driven scenario, which is illustrated in Fig. 7(a), the corresponding correction $\delta|a|^2$ in our proposed doubly driven scenario can be suppressed to a very low level as in Fig. 7(b). For our used sideband intensity in the measurement, the thermal noise existing at different temperatures only slightly modifies it; see Fig. 5.

V. EXPERIMENTAL FEASIBILITY

Previously, a different two-pump scenario was implemented by detuning two drive tones from the cavity resonant

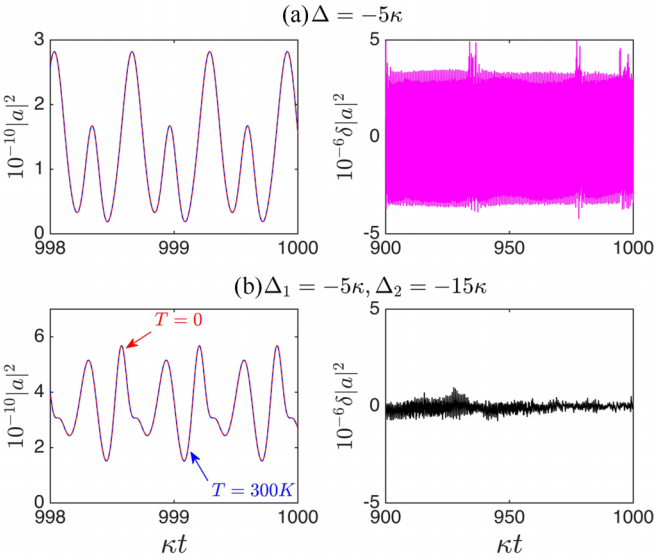

FIG. 7. The evolved intracavity photon number $|a|^2$ and the corresponding correction $\delta|a|^2$ by the thermal noise at the room temperature $T = 300$ K. In the left frames, the red curve is for $T = 0$ and the blue dashed one is for $T = 300$K. In (a) the system is driven by a single field detuned at $\Delta/\kappa = -5$, while in (b) the system is driven by two fields with $\Delta_1 = -5\kappa$, $\Delta_2 = -15\kappa$, respectively. The mechanical quality factor is fixed to be $Q = 10^4$ and the drive amplitude is $E = 10^6\kappa$. The other fixed parameters are the same as those in Fig. 2.

frequency ω_c^0 to $\omega_c^0 + \omega_m$ and $\omega_c^0 - \omega_m$, respectively, realizing a different type of dynamical instability [39]. The basic techniques in that experiment are applicable to the current scheme. One flexibility to the current scheme is that only the condition in Eq. (7) is the most essential; that is, to keep the frequency difference between the two tones to be as close to the mechanical frequency as possible. Despite the different performance at the different working points as shown in Fig. 6, the concerned dynamical behaviors can be always realized by an adjustment of driving laser power, as long as such a frequency difference can be maintained. The acousticoptic modulator (AOM) [40] or single-sideband modulator (SSB) [41]) can be applied to adjust the drive frequencies to approach the condition.

Certainly it is ideal to have two completely stable driving laser frequencies to avoid the indistinguishably of the frequency shift by the external force from the laser frequency shifts themselves. It is possible to apply the PDH technique for stabilizing laser frequencies [34–36]. Compared with the other schemes based on PDH or other techniques mentioned in Introduction, the effect of thermal noise can be negligible in our approach. With regard to the feasibility with the current experimental technology, our scheme is a workable alternative to force sensing.

VI. SUMMARY

By an example of pumping an optomechanical system by a two-tone field with properly matched frequencies, we present a detailed description of an approach to weak force sensing. Different from previous proposals, the setup works with a nonlinear dynamical mechanism, which induces a measurable change of the cavity-field sidebands in the presence of an external weak force to be measured. Instead of determining the cavity frequency shift by the external force, we realize a detectable amplitude change in the cavity-field spectrum by such a system manifesting a fully locked mechanical oscillation. The cavity-field modification upon its transition between two locked patterns associated with the locked mechanical oscillation provides a possible way of force sensing. The setup is relatively simple without a more complicated structure, but the requested sensitivity can be achieved with a robustness against thermal perturbation. The sensitivity to the level of attonewton is achievable with the currently available experimental conditions. These features considerably relax the setup requirement on force sensing to a very tiny level.

ACKNOWLEDGMENTS

The authors thank Dr. Yan Lei Zhang and Dr. Zhen Shen for the helpful discussions. This work was supported by National Natural Science Foundation of China (Grant No. 11574093), Natural Science Foundation of Fujian Province of China (Grant No. 2020J01061), and ANID Fondecyt Regular (1221250).

[1] C. L. Degen, F. Reinhard, and P. Cappellaro, Quantum sensing, Rev. Mod. Phys. **89**, 035002 (2017).
[2] B. B. Li, L. F. Ou, Y. C. Lei, and Y. C. Liu, Cavity optomechanical sensing, Nanophotonics **10**, 2799 (2021).
[3] J. Chaste, A. Eichler, J. Moser, G. Ceballos, R. Rurali, and A. Bachtold, A nanomechanical mass sensor with yoctogram resolution, Nat. Nanotechnol. **7**, 301 (2012).
[4] M. R. Foreman, J. D. Swaim, and F. Vollmer, Whispering gallery mode sensors, Adv. Opt. Photon. **7**, 168 (2015).
[5] X. F. Jiang, C. L. Zou, L. Wang, Q. H. Gong, and Y. F. Xiao, Whispering-gallery microcavities with unidirectional laser emission, Laser Photonics Rev. **10**, 40 (2016).
[6] F. Vollmer and S. Arnold, Whispering-gallery-mode biosensing: label-free detection down to single molecules, Nat. Methods **5**, 591 (2008).
[7] J. G. Zhu, S. K. Ozdemir, Y. F. Xiao, L. Li, L. N. He, D. R. Chen, and L. Yang, On-chip single nanoparticle detection and sizing by mode splitting in an ultrahigh-Q microresonator, Nat. Photonics **4**, 46 (2010).
[8] L. B. Shao, X. F. Jiang, X. C. Yu, B. B. Li, W. R. Clements, F. Vollmer, W. Wang, Y. F. Xiao, and Q. H. Gong, Detection of single nanoparticles and lentiviruses using microcavity resonance broadening, Adv. Mater. **25**, 5616 (2013).
[9] E. Gavartin, P. Verlot, and T. J. Kippenberg, A hybrid on-chip optomechanical transducer for ultrasensitive force measurements, Nat. Nanotechnol. **7**, 509 (2012).
[10] J. Moser, J. Güttinger, A. Eichler, M. J. Esplandiu, D. E. Liu, M. I. Dykman, and A. Bachtold, Ultrasensitive force detection with a nanotube mechanical resonator, Nat. Nanotechnol. **8**, 493 (2013).

[11] S. Schreppler, N. Spethmann, N. Brahms, T. Botter, M. Barrios, and D. M. Stamper-Kurn, Optically measuring force near the standard quantum limit, Science **344**, 1486 (2014).
[12] D. Mason, J. Chen, M. Rossi, Y. Tsaturyan, and A. Schliesser, Continuous force and displacement measurement below the standard quantum limit, Nat. Phys. **15**, 745 (2019).
[13] O. Arcizet, T. Briant, A. Heidmann, and M. Pinard, Beating quantum limits in an optomechanical sensor by cavity detuning, Phys. Rev. A **73**, 033819 (2006).
[14] M. Tsang and C. M. Caves, Coherent Quantum-Noise Cancellation for Optomechanical Sensors, Phys. Rev. Lett. **105**, 123601 (2010).
[15] X. N. Xu and J. M. Taylor, Squeezing in a coupled two-mode optomechanical system for force sensing below the standard quantum limit, Phys. Rev. A **90**, 043848 (2014).
[16] F. Bariani, H. Seok, S. Singh, M. Vengalattore, and P. Meystre, Atom-based coherent quantum-noise cancellation in optomechanics, Phys. Rev. A **92**, 043817 (2015).
[17] A. Motazedifard, F. Bemani, M. H. Naderi, R. Roknizadeh, and D. Vitali, Force sensing based on coherent quantum noise cancellation in a hybrid optomechanical cavity with squeezed-vacuum injection, New J. Phys. **18**, 073040 (2016).
[18] L. F. Buchmann, S. Schreppler, J. Kohler, N. Spethmann, and D. M. Stamper-Kurn, Complex Squeezing and Force Measurement Beyond the Standard Quantum Limit, Phys. Rev. Lett. **117**, 030801 (2016).
[19] S. M. Huang and G. S. Agarwal, Robust force sensing for a free particle in a dissipative optomechanical system with a parametric amplifier, Phys. Rev. A **95**, 023844 (2017).
[20] W. Z. Zhang, Y. Han, B. Xiong, and L. Zhou, Optomechanical force sensor in a non-Markovian regime, New J. Phys. **19**, 083022 (2017).
[21] A. Motazedifard, A. Dalafi, F. Bemani, and M. H. Naderi, Force sensing in hybrid Bose-Einstein-condensate optomechanics based on parametric amplification, Phys. Rev. A **100**, 023815 (2019).
[22] D. N. Bernal-García, H. Vinck-Posada, and M. J. Woolley, Non-stationary force sensing under dissipative mechanical quantum squeezing, Phys. Rev. A **102**, 053515 (2020).
[23] W. J. Gu, Y. Y. Wang, Z. Yi, W. X. Yang, and L. H. Sun, Force measurement in squeezed dissipative optomechanics in the presence of laser phase noise, Opt. Express **28**, 12460 (2020).
[24] Y. H. Zhou, Q. S. Tan, X. M. Fang, J. F. Huang, and J. Q. Liao, Spectrometric detection of weak forces in cavity optomechanics, Opt. Express **28**, 28620 (2020).
[25] S. Davuluri, Quantum optomechanics without the radiation pressure force noise, Opt. Lett. **46**, 904 (2021).
[26] S. L. Chao, Z. Yang, C. S. Zhao, R. Peng, and L. Zhou, Force sensing in a dual-mode optomechanical system with linear-quadratic coupling and modulated photon hopping, Opt. Lett. **46**, 3075 (2021).
[27] F. Bemani, O. Černotík, L. Ruppert, D. Vitali, and R. Filip, Force Sensing in an Optomechanical System with Feedback-Controlled in-Loop Light, Phys. Rev. Appl. **17**, 034020 (2022).
[28] A. N. Xu and Y. C. Liu, Optomechanically enhanced precision measurement, Phys. Rev. A **106**, 013506 (2022).
[29] C. W. Gardiner and P. Zoller, *Quantum Noise* (Springer Verlag, 2000).
[30] Q. Lin, B. He, and M. Xiao, Entangling Two Macroscopic Mechanical Resonators at High Temperature, Phys. Rev. Appl. **13**, 034030 (2020).
[31] Q. Lin, B. He, and M. Xiao, Mass sensing by detecting the quadrature of a coupled light field, Phys. Rev. A **96**, 043812 (2017).
[32] F. Marquardt, J. G. E. Harris, and S. M. Girvin, Dynamical Multistability Induced by Radiation Pressure in High-Finesse Micromechanical Optical Cavities, Phys. Rev. Lett. **96**, 103901 (2006).
[33] M. Aspelmeyer, T. J. Kippenberg, and F. Marquardt, Cavity optomechanics, Rev. Mod. Phys. **86**, 1391 (2014).
[34] R. V. Pound, Electronic frequency stabilization of microwave oscillators, Rev. Sci. Instrum. **17**, 490 (1946).
[35] R. W. P. Drever, J. L. Hall, F. V. Kowalski, J. Hough, G. M. Ford, A. J. Munley, and H. Ward, Laser phase and frequency stabilization using an optical resonato, Appl. Phys. B **31**, 97 (1983).
[36] E. D. Black, An introduction to Pound-Drever-Hall laser frequency stabilization, Am. J. Phys. **69**, 79 (2001).
[37] B. He, Q. Lin, M. Orszag, and M. Xiao, Mechanical oscillations frozen on discrete levels by two optical driving fields, Phys. Rev. A **102**, 011503(R) (2020).
[38] Y. Wu, G. Li, B. He, and Q. Lin, Amplitude and phase locking of mechanical oscillation driven by radiation pressure, Phys. Rev. A **105**, 013521 (2022).
[39] I. Shomroni, A. Youssefi, N. Sauerwein, L. Qiu, P. Seidler, D. Malz, A. Nunnenkamp, and T. J. Kippenberg, Two-Tone Optomechanical Instability and Its Fundamental Implications for Backaction-Evading Measurements, Phys. Rev. X **9**, 041022 (2019).
[40] P. Verlot, A. Tavernarakis, T. Briant, P.-F. Cohadon, and A. Heidmann, Backaction Amplification and Quantum Limits in Optomechanical Measurements, Phys. Rev. Lett. **104**, 133602 (2010).
[41] Z. Shen, Y.-L. Zhang, C.-L. Zou, G.-C. Guo, and C.-H. Dong, Dissipatively Controlled Optomechanical Interaction via Cascaded Photon-Phonon Coupling, Phys. Rev. Lett. **126**, 163604 (2021).